Available online at www.sciencedirect.com

ScienceDirect

Advances in Space Research 56 (2015) 1146–1160

ADVANCES IN SPACE RESEARCH (a COSPAR publication)

www.elsevier.com/locate/asr

Ground track density considerations on the resolvability of gravity field harmonics in a repeat orbit

J. Klokočník [a,*], C.A. Wagner [b], J. Kostelecký [c], A. Bezděk [a]

[a] Astronomical Institute, Czech Academy of Sciences (ASÚ), CZ – 251 65 Ondřejov Observatory, Czech Republic
[b] 2801 Roesh Way, Vienna, VA 22181, USA
[c] Research Institute of Geodesy, Topography and Cartography (VÚGTK), CZ – 250 66 Zdiby and TU Ostrava, CZ – 708 33 Ostrava-Poruba, Czech Republic

Received 6 January 2015; received in revised form 16 June 2015; accepted 18 June 2015
Available online 25 June 2015

Abstract

One of the limiting factors in the determination of global gravity field parameters is the spatial sampling, namely during phases when the satellite is in an orbit with few revolutions for each repeat cycle. This often happens when it is freely passing (drifting) through the atmosphere and encountering a fair number of such deficient repeat orbits. This research was triggered in 2004 by the significant but only temporary, 2–3 months long, decrease of the accuracy of monthly solutions for the gravity field variations derived from GRACE. The reason for the dip was the 61/4 resonance in the GRACE orbits in autumn 2004. At this resonance, the ground track density dramatically decreased and large (mainly longitude) gaps appeared in the data-coverage of the globe. The problem of spatial sampling has been studied repeatedly (Wagner et al., 2006; Klokočník et al., 2008; Weigelt et al., 2009) and simple rules have been derived to limit the maximum order for unconstrained solutions (inversions) for the gravity field parameters or their variations from observations of a single satellite. Here we work with the latest rule from Weigelt et al. (2013) which distinguishes the maximum attainable order according to the parity of the two parameters defining the repeat orbit or orbital resonance, β the number of nodal satellite's revolutions in α nodal days (α, β co-prime integers, the ratio β/α irreducible). This rule, that the resolvable order (in a repeat near polar orbit) should be β for odd parity ($\beta - \alpha$) and $\beta/2$ for even parity ($\beta - \alpha$) orbits, arose from the discovery that the number of distinct and equally spaced equatorial crossings (ascending and descending passes) for odd parity ($\beta - \alpha$) is 2β while for even parity orbits it is only β. We extend this insight over all achievable latitudes and assess the ground track density (or coverage) by way of the maximum distances between subsatellite points at arbitrary latitude, specifically for the nearly polar (drifting) orbits of CHAMP, GRACE, and the repeat tuned GOCE. We demonstrate clearly how latitude (and also the orbital inclination) is important and affects the choice of an order resolution limit. A new rule, compromising between β and $\beta/2$ for each specific repeat orbit, is proposed, based on the average maximum distance between subsatellite points over the achievable latitudes. Although these findings allow an initial estimate of recoverability based solely on the global spatial sampling of the ground track, a more refined analysis involving the inversion of specific observations is still outstanding.

Keywords: Gravity field of the Earth; Resonant/repeat orbit missions; Ground track density; Resolvability; Maximum degree/order limit

1. Introduction, motivation, and aim of this work

Time series of changes of the gravity field can be derived, as successfully demonstrated mainly by the satellite mission GRACE (e.g., Bettadpur et al., 2004; Lemoine et al., 2007). The changes are due to mass

* Corresponding author.
E-mail addresses: jklokocn@asu.cas.cz (J. Klokočník), carl.wagner2@verizon.net (C.A. Wagner), kost@fsv.cvut.cz (J. Kostelecký), bezdek@asu.cas.cz (A. Bezděk).

http://dx.doi.org/10.1016/j.asr.2015.06.020
0273-1177/

redistribution (ice, continental water, sea level, etc.) in the Earth system and are therefore of great relevance to climate research. However, the characteristics of each of the gravity maps in terms of accuracy and spatial resolution are not identical. If the orbit of the satellite is freely drifting, many repeat orbits will occur with the possibility of much coarser ground track patterns. In the literature several "rules" have been formulated expressing the aimed-for spatial resolution in terms of the maximum possible degree or order. The current M_{max}-rules were derived from an analysis of the pattern of ground track equator crossings of the ascending and descending arcs.

While these rules are solely based on the pattern of equator crossings (Wagner et al., 2006; Klokočník et al., 2008; Weigelt et al., 2009, 2013), the present work takes into account a possible latitude (and inclination) dependence. The authors here analyze the actual ground track patterns of CHAMP, GRACE and GOCE over all their available latitudes and then derive a more general rule for M_{max}.

Today, we infer that the ground track density of a repeat orbit configuration limits the recovery resolution of gravity (static or variable) from observations on that orbit. It may be feasible to solve for gravity parameters above a reasonable maximum limit in degree and/or order of harmonic expansion of the geopotential, but such a solution may not be correct from a physical viewpoint: it may require external information. It was anticipated for a long time that there must exist such a track density-Nyquist-type limit on spherical harmonic resolution and indeed Colombo (1984a,b) presented one based only on a minimally correlated inversion matrix. [The simplest rationale for Colombo's (Nyquist-type) rule is the fact that an orbit with β revolutions has β equally space ascending arcs in each repeat cycle. We will expand on this insight in what follows.] Colombo's rule states that a (band limited) gravity field recovery up till degree L_{max} = order M_{max} from a resonant (repeat) orbit requires at least $2L_{max}$ revolutions. The practical experience of gravity field recovery from various authors, however, does not support this rule (Weigelt et al., 2009, 2013; Visser et al., 2012 and many experiments performed in the Astronomical Institute, Ondřejov, at NOAA, Silver Spring and in Faculté des Sciences, de la Technologie et de la Communication). The rule looks too stringent.

In this work we speak about the spatial resolution for the nearly polar orbits of CHAMP, GRACE and GOCE only. The critical component is not that along the orbit where the sampling depends on the frequency of the measuring instruments on board and is usually more than sufficient for the recovery desired. The spatial problem comes in the "cross-track" component, de facto in longitude, and this is related to the maximum resolvable *order* of harmonics M_{max}. [Note also that here we are concerned only about spatial sampling as a clue to resolvability, not time undersampling (e.g., Visser et al., 2010)]. We recall the situation of GRACE and its orbit resonance $\beta/\alpha = 61/4$ (61 nodal revolutions during 4 nodal days of return to the same geographic starting node; for more details see below, Section 2.1.) The precision of monthly solutions for gravity fields of L_{max}, $M_{max} = 120, 120$, derived from GRACE data by various authors (e.g., Bettadpur et al., 2004; Tapley et al., 2004; Lemoine et al., 2007), temporarily decreased in autumn 2004, as is shown in Fig. 1. At that time this dramatic drop in precision of the gravity field products without obvious reasons was not expected. The same type and quality of observations, their processing, etc. were used during the whole tested period. It was explained by the influence and impact of the 61/4 repeat orbit (Wagner and McAdoo, 2004; Wagner et al., 2006). GRACE, freely decaying in the atmosphere, encountered various orbit repeat conditions and this low order 61/4 repeat had an enormous effect (unfortunately negative and fortunately only for a few months) on the quality of the (120, 120) gravity solutions derived from GRACE measurements near that time. A similar gravity degradation

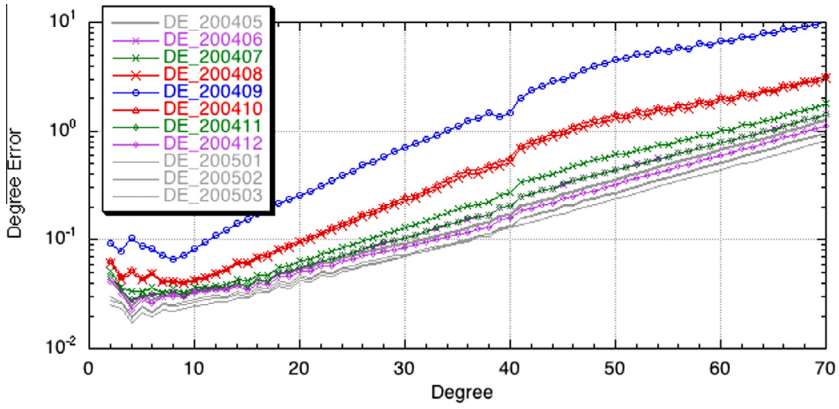

Fig. 1. Precision of monthly solutions for the gravity field variations, derived from the GRACE data, temporarily decreased in the vicinity of the 61/4 repeat orbit (see the red curves for months 08 and 10 in year 2004 and the blue curve for 09/2004). Note the logarithmic scale on the y-axis. No external constraints for non-zonals were used in these solutions. Original figure from 2004; courtesy Bettadpur et al. (2004). (For interpretation of the references to color in this figure legend, the reader is referred to the web version of this article.)

occurred for CHAMP (Reigber et al., 2002) passing through the 31/2 repeat orbit many times because of intentional orbit maneuvers.

Wagner et al. (2006) supported the "Colombo rule" by their own derivation when studying ideal and degraded geopotential resolution. They proved this rule guaranteed a unique resolution of same order, m, degree, l, parity and kind (C_{lm} or S_{lm}) from observable along-track wave phases within the repeat period α, uncorrelated with other geopotential harmonics. It is interesting and important to note how many "remote sensing people" and others became well aware of the fact that sparse ground track coverage due to the changing orbit configuration has a severe impact on the quality of fixed resolution results derived from measurements taken from satellites in such orbits. Since Wagner et al. (2006), more than 30 references have elaborated on it, e.g., Awange et al. (2008), Bettadpur (2008), Elsaka et al. (2014), Ramillien et al. (2011, 2012), Save et al. (2012), Seitz et al. (2008), Schmidt et al. (2008), Swenson et al. (2006), Weigelt et al. (2008, 2010), Wiese et al. (2012), Zaitchik et al. (2008).

We show the ground track density decrease at the low order 61/4 repeat in contrast to the situation "far" from it (Fig. 2a and b). The difference in the track density between these two cases is directly projected into a degradation of quality of the monthly gravity solutions from the "normal" situation (Fig. 2a) to the situation near the exact repeat condition (Fig. 2b), as demonstrated by the error spectra in Fig. 1.

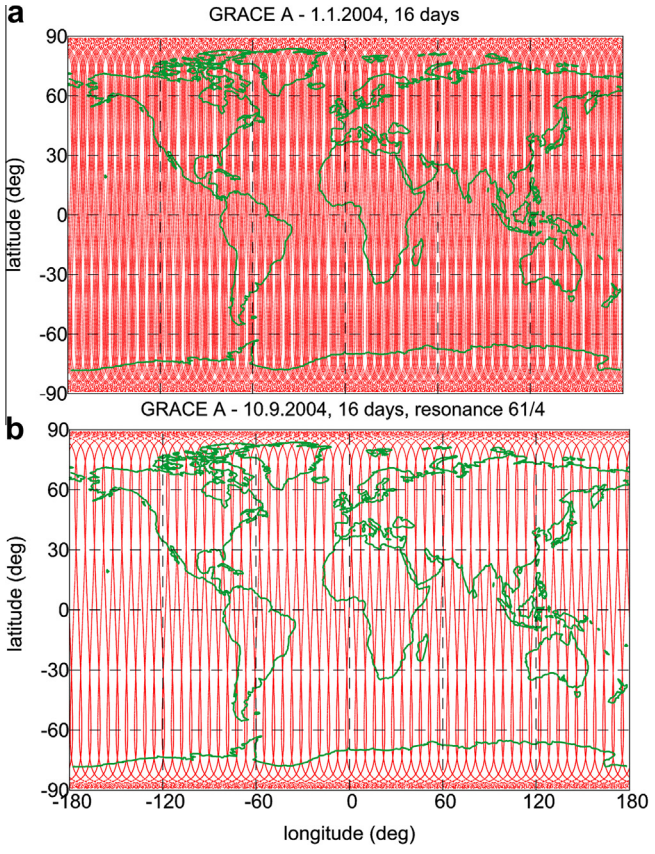

Fig. 2. (a) Ground-tracks of GRACE A a few months before the 61/4 repeat orbit (situation in January 2004) and (b) at the exact 61/4 repeat (September 2004). This track density difference correlates with the accuracy changes of the monthly solutions derived from data on GRACE A/B, as is shown in Fig. 1 (reproduced from Klokočník et al., 2008).

Klokočník and Kostelecký (2006) and Klokočník et al. (2008) studied low order repeat orbit effects on the quality of results from CHAMP, GRACE, and GOCE. They estimated – as a warning – that future passes of GRACE satellites through further deficient orbit-repeats (as the 31/2 in 2015) will inevitably suffer degradation in gravity recovery around them. Visser et al. (2012) suggested a new rule, for single satellite geodetic missions like CHAMP, GRACE, and GOCE, namely $L_{max} < \beta$. Here we show how this relaxation of "Colombo rule" is directly related to an increase in track coverage beyond the strict requirements of that rule.

Weigelt et al. (2013), Eqs. (18a,b), recommended a refinement for the rule defining the recoverable M_{max} from measurements on a single satellite in a repeat orbit.

$$M_{max} < \beta \quad \text{for } (\beta - \alpha) \ \ldots \ \text{odd}, \tag{1a}$$

$$M_{max} < \beta/2 \quad \text{for } (\beta - \alpha) \ \ldots \ \text{even}. \tag{1b}$$

(i) The fact that M_{max} depends on order β is not new (the higher β, the better coverage, in turn potentially smaller errors of harmonic geopotential coefficients derived, all other factors being equal). But (ii) the rule (1a,b) introduces dependence of maximum order on the parity of the repeat orbit difference $(\beta - \alpha)$, whether it is the same or opposite. (iii) The new rule should be valid for orbits of arbitrary but near polar inclinations since a significant lack of data away from the poles will compromise any global geopotential solution no matter how dense the coverage is within the orbit's accessible latitudes. However, as we shall see in the next section both the Weigelt and the old Colombo rules for resolvable maximum order reflect only the track coverage on the equator. Our objective is to extend these insights to reflect the track coverage over all available latitudes.

(Note that we do distinguish here between effects caused by the polar gap phenomenon and the gaps between neighboring arcs. Both are effects caused by an insufficient sampling but the former affects mostly the zonal and near-zonal coefficients which we assume will be negligible for a near polar orbit).

To assess the 'density' of coverage 'globally' we examine the maximum distance between adjacent ascending and descending arcs at each latitude and compute its average over all the latitudes seen by the orbit (following Klokočník et al., 2008). (Note that these conveniently found maximum distances are inversely related to track 'density' coverage: where they are greater the coverage is less, where they are smaller the coverage is greater).

For example below in Fig. 3 we plot the distance of ground tracks for GRACE using the actual orbital data (mean NASA two-line elements available usually once

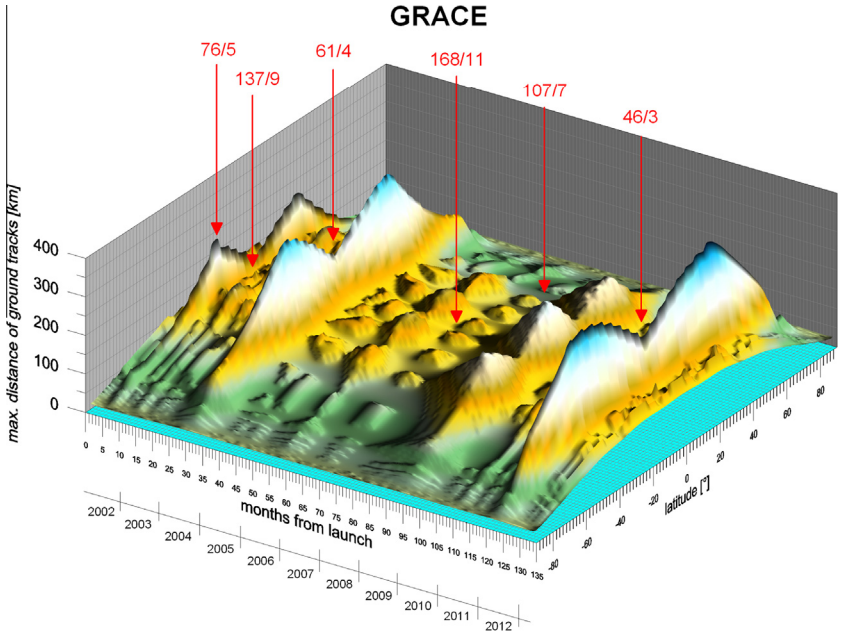

Fig. 3. 3D graph of evolution of ground track "density" for GRACE. Maximum distance of the ground tracks is plotted as a function of time and latitude. Important repeat orbits are marked. Computed with NASA two-line elements. The longest distance between the ground tracks is not always at the equator, as might be expected (see also Fig. 4a–f). The greatest distances are at the equator when $(\beta - \alpha)$ is even and the shortest when $(\beta - \alpha)$ is odd, as expected from the Weigelt rule (Eqs. (1a,b)). Observe how narrow the intervals of the low density around the low order repeat orbits are (typically 1–3 months), in comparison with other intervals, and how irregular (in time) the distribution of the low order resonant regimes is during the satellite's lifetime.

per day). Later (in Section 2.5) we will compare these "observed" densities with "theoretical densities" (Fig. 10).

Note the maximum distances in Fig. 3 depends on the parity $(\beta - \alpha)$ as well as on the latitude. For example, supporting the distinction in Eqs. (1a,b) [from Weigelt et al., 2013], for orbits of roughly the same altitude [77/5 vs 78/5, and 46/3 vs 47/3] the greater maximum distances (less dense coverage) occur for these resonances where the parity of $(\beta - \alpha)$ is even.

Now, we take GRACE and the six resonances marked in Fig. 3 as an example. We plot the maximum ground track distances/density for them (from the actual orbital data, see the series in Fig. 4a–f). We can compare the resolvability limit (according to Eqs. (1a,b)) and the density of the ground tracks at the equator. The results are summarized in Table 1. For $(\beta - \alpha)$ odd (the examples for the 76/5, 61/4, 168/11, 46/3 repeats) we see higher density of ground tracks at the equator than in the surrounding equatorial zones (say at $|\varphi| = 30°$). For these the rule (1a) recommends $M_{max} < \beta$. While for $(\beta - \alpha)$ even, the cases 137/9 and 107/7 show higher density at non-zero (but low) latitudes $|\varphi|$, here (for $I = 89°$) roughly at 15°, and the rule (1b) recommends that $M_{max} < \beta/2$.

Fig. 5 shows the formal standard deviations of the GRACE GFZ solutions (Release 05a) in terms of geoid height for the peak months of the repeat cases of Table 1. The cases of September 2012, December and January 2013 are unaffected by low-order repeat orbits and added for reference. A degradation due to the orbit configuration is visible. The smallest degradation occurs for December 2006 for the repeat period of 168/11 which has the largest predicted resolvability limit M_{max} of all the solutions shown in Table 1. The higher the number of orbits in a repeat cycle, the denser will be the sampling and the degradation smaller. Note that this figure is based on formal errors. The true errors may deviate for various reasons. Furthermore, other effects such as missing data may also deteriorate the quality of the solution.

GOCE (Floberghagen et al., 2011) was launched in 2009 and decayed in 2013. It was held (by fine orbit tuning) in specific high order resonance/repeat orbits using the resonant evolution graph (like that in Fig. 6) which were pre-selected (by ESA) for optimum gravity field determination (ESA, 1999, 2014; Bezděk et al., 2009, 2010). The following orbits (Table 2) were chosen and kept temporarily in these repeat orbits during its decay (Floberghagen, priv. commun., 2013; ESA, 2014) by means of an ion motor on board of GOCE (with precision of about ±5 m in height).

From the actual NASA two-line mean elements of GOCE, we show its mean motion in Fig. 7. Initially GOCE freely decayed from height of about 280 km, then was stabilized in the 979/61 repeat at a height of 255 km. When the height is constant, the gradiometric measurements may work well; when variable, the orbit maneuver from one to another repeat (Table 1) took place or a multifunction in the maneuver system may have occurred. The most serious problem appeared for August–September 2010 (see ESA, 2014).

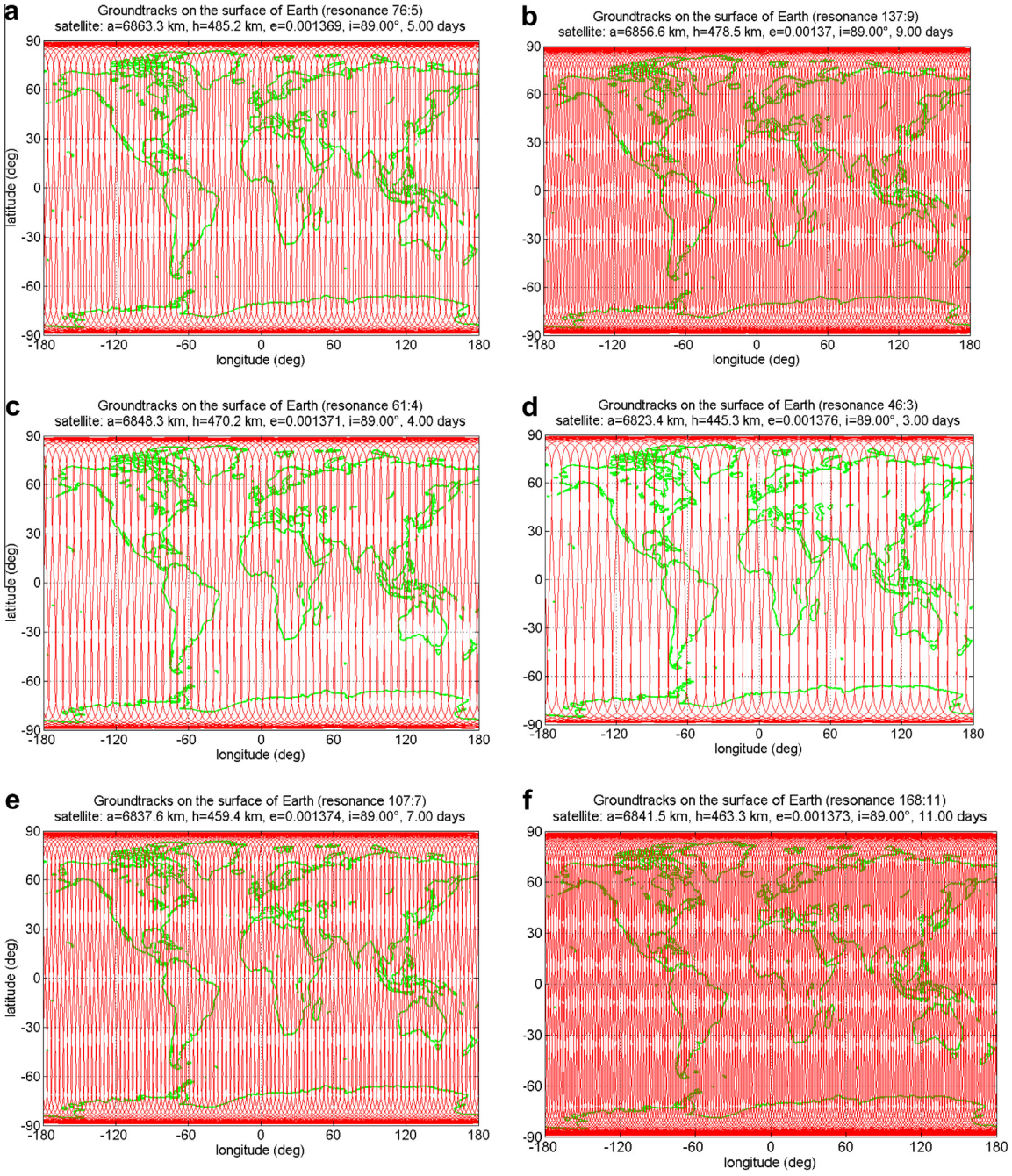

Fig. 4. (a–f) Ground tracks of GRACE at the exact repeat orbits marked in Fig. 3, *a* for the 76/5, *b* for 137/9, *c* for 61/4, *d* for 168/11, *e* for 107/7, and *f* for 46/3.

Table 1
Ground track density and suggested resolvability limits for GRACE (Eqs. (1a,b)).

Repeat orbit	$(\beta - \alpha)$	M_{max}	Equator crossing *asc.– desc. track*	Time
76/5	Odd	75	Full density	September 2002
137/9	Even	68	~Half density	April 2003
61/4	Odd	60	Full density	September 2004
168/11	Odd	167	Full density	December 2006
107/7	Even	53	~Half density	December 2009
46/3	Odd	45	Full density	June 2012
31/2	Odd	30	Full density	March 2015

Note that the fine orbit tuning of GOCE was possible only due to its on-board ion motor. But a choice of orbit repeat or avoidance of a specific 'repeat' to fulfil various requirements of satellite missions was important for altimetry satellites (e.g., Reigber et al., 1988) and is important for new satellites (like bistatic altimetry with GNSS, Klokočník et al., 2011) as well as for planetary missions to study gravity fields of the celestial bodies (Klokočník et al., 2010).

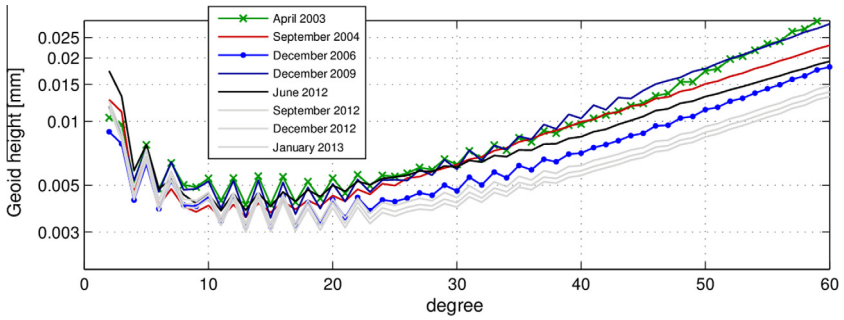

Fig. 5. Precision of the monthly gravity field solutions derived from GRACE data temporarily decreased in the vicinity of the orbit-repeats of Table 1. Note the logarithmic scale on the y-axis. Courtesy M. Weigelt.

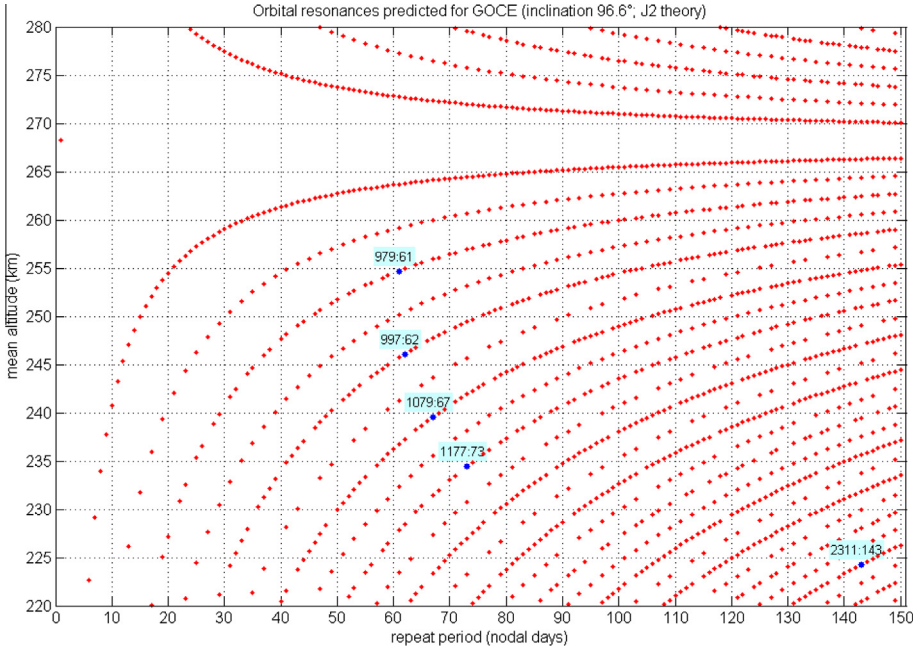

Fig. 6. "Repeat orbit evolution graph" for GOCE and the repeat orbits selected for the gradiometric measurements. The repeat cycle choices are driven by the desire to optimize the spatial coverage by the GOCE gradiometer measurements.

Table 2
Actual selected resonant orbits for gradiometry measurements of GOCE, fine orbit tuning.

Repeat orbit β/α	Height [km]	Duration
979/61	255	About 3 first years of operations
997/62	246	1 Cycle in Sep/Oct 2012
1079/67	240	1 Cycle in Dec 2012/Jan 2013
1177/73	235	1 Cycle in March/April 2013
2311/143	224	From early June 2013 till the decay

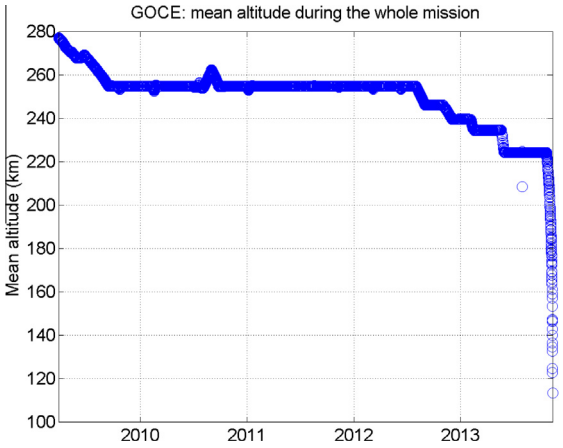

Fig. 7. Mean altitude of GOCE from NASA two-line elements during its whole lifetime.

2. Prerequisities for a generalization of the rule for the limit M_{max}

2.1. Definition of orbital resonance for the Earth's artificial satellites

The exact condition for commensurability is that the satellite is in the exact β/α orbital resonance when it performs β revolutions or nodal periods (from one orbital

node to the next node (of the same type) while the Earth rotates α times with respect to the precessing orbit plane (known also as nodal days); α, β are prime integers, the ratio β/α is irreducible. After this interval the path of the satellite relative to the Earth repeats exactly, which is the physical reason for the resonance effect (Gooding, 1971; Allan, 1973; review in Klokočník et al., 2013). *Repeat orbit* is here a manifestation of phenomenon of *orbit resonance*.

2.2. The mean motion of a satellite in a repeat orbit (resonance) over a rotating ellipsoid

The third Kepler law for the Earth represented by a mass point or a homogeneous sphere or a sphere homogeneous in spherical layers is

$$n_0^2\, a^3 = GM, \tag{2}$$

with the mean motion $n_0 = 2\pi/T$, where T is the sidereal orbit period, a the mean semimajor axis, and GM is the product of the universal gravitational constant G and the mass M of the Earth (GM is known also as the geocentric gravitational constant); the mass of the satellite is assumed to be negligible.

A modified or generalized mean motion $n(J_2)$ in the case of orbital resonance and for the Earth represented by a (geocentric) rotational ellipsoid (Klokočník et al., 2003) is:

$$n = \frac{\beta}{\alpha}|\dot{S}|\left\{1 - \frac{3}{2}J_2\left(\frac{R}{a}\right)^2\left(4\cos^2 I - \frac{\beta}{\alpha}\cos I - 1\right)\right\}, \tag{3}$$

where $\dot{S}$ is the time derivative of the sidereal angle, i.e., rotational speed of the Earth (1.00274 rev/day), R is the semimajor axis of the Earth's reference ellipsoid or a radius of a reference sphere (we use 6371 km), the gravitational field is approximated by only the first zonal (fully normalized) harmonic coefficient $J_2 = -\sqrt{5}\,\bar{C}_{20}$ and I is the orbital inclination. It is useful to note that the orbital period Δt for a β/α repeat orbit from (3) is Δt [days] $= I$[rev]/n[rev/day]. The mean motion (3) can then be rewritten approximately as $n_0 = \beta/\alpha\,(|\dot{S}|)$, thus

$$\alpha/\beta \approx 1/n_0. \tag{4}$$

2.3. Distance between ascending and descending tracks at the equator

We now derive a theoretical formulae for the distance between ascending and descending tracks at an arbitrary latitude.

Given a β/α exact repeat (resonant) orbit (mission). In it, there are exactly $360°/\beta$ equally spaced positions for ascending and the same number for descending longitude nodes around the equator. Assume a non-equatorial orbit (in reality we consider only nearly-polar orbits of CHAMP, GRACE, and GOCE, as mentioned above).

Assume that the first ascending node has a longitude of zero degrees on the equator, $d^{eq}_{asc} = 0$. Denote the first descending longitude as d^{eq}_{desc}. What is the distance the Earth rotates in the time it takes for 1/2 a revolution of the satellite, i.e., $\Delta t/2$ when it first crosses the equator on a descending pass? That rotation distance will be 360 (the Earth's rate in degrees/day) times α/β times 1/2. Thus the geographic longitude difference between the first ascending and descending node is:

$$d^{eq}_{asc} - d^{eq}_{desc} = 0^\circ + 180^\circ - 180^\circ(\alpha/\beta)^\circ = 180^\circ(1 - \alpha/\beta)$$
$$= \pi(1 - \alpha/\beta),$$

already known to Weigelt et al. (2013), where 180° corresponds to π in radians.

Let N be the positive integer of the equally spaced ascending nodes on the equator closest to the longitude of the first descending node; its longitude will be $360°\ N/\beta$. Also let f be a fraction ($0 \leqslant f \leqslant 1$) of the longitude spacing of the ascending crossings $360°/\beta$ marking the position of a descending crossing relative to its two neighboring ascending equator crossings. Then the distance between the equatorial ascending node closest to the first descending crossing is:

$$f(360/\beta) = \pi(1 - \alpha/\beta) - 2\pi N/\beta \quad \text{or}$$
$$f = (1/2)[\beta - \alpha - 2N], \tag{5}$$

thus $2f = (\beta - \alpha - 2N)$ is an integer. For $2f$ to be an integer, since f is between 0 and 1, f can only be either 0, 1 or 1/2. The first two possibilities imply all the descending equator crossings are at the same location as the ascending. In addition (for these cases) $\beta - \alpha$ must be *even* since $2f$ is also *even* then and $2N$ always is even. Similarly if f is 1/2, $2f$ is *odd* (=1) and $\beta - \alpha$ must also be *odd*. For that case all the descending equatorial crossings fall exactly midway between their neighboring ascending ones.

In summary, for equatorial coverage, repeat orbits with $(\beta - \alpha)$ *odd* yield twice the track density as orbits with $(\beta - \alpha)$ of *even* parity. Further, for both repeat orbit parities the adjacent crossings are regularly spaced and strongly suggest a Nyquist-type rule for M_{max} if these coverage conditions existed at all available latitudes (Eqs. (1a,b)). But in fact these Nyquist-type conditions do *not* exist at all these other latitudes which motivated us to compromise Eqs. (1a,b) according to how closely the actual repeat orbit agreed with the "ideal" of equal spacing between adjacent crossings at all such latitudes. For a few examples see Table 1 and Figs. 2a, b; 3 and 4a–f; 10, 14a–e.

We note that, providing the advantages of orbits with $\beta - \alpha$ of odd parity persist at other latitudes, such repeat conditions yield superior global coverage and by extension higher M_{max} will be about twice as frequent as repeat orbits of even parity $\beta - \alpha$ because repeat orbits of both β and α even cannot exist (since their β/α would be reducible).

In the next section we use the maximum distance between adjacent crossings at each latitude to assess how closely the given orbit comes to the two extremes for this spacing, $180/\beta$ for the densest (yielding $M_{max} = \beta$), or $360/\beta$ (yielding $M_{max} = \beta/2$).

2.4. Maximum distance d_{max} between subsatellite points at arbitrary latitude in β/α repeat orbits

Density (*or* Spacing) *of ground tracks* – Spacing (of the ground tracks) will be defined here by the distances between an ascending and its nearest descending ground track, i.e., by Eq. (12) below.

The final aim of derivation in this section is to find the maximum distance d_{max} of ground tracks crossing a parallel φ corresponding to the β/α resonance. Assume (1) a circular orbit, (2) that the Earth is represented by a sphere with radius R, and (3) we neglect orbit precession due to C_{20}. In the spherical right triangle for mean anomaly M, orbital inclination I and latitude φ, the law of sines yields (Kaula, 1966; Rosborough, 1986):

$$\sin M = \frac{\sin\varphi}{\sin I}. \tag{6}$$

We recall Eq. (4); the orbital period Δt for a β/α repeat orbit is

$$\Delta t = \frac{1}{n_0} = \frac{\alpha}{\beta}.$$

First, we seek a distance Δ_{asc} between two neighboring ascending tracks for two points at the same latitude φ after interval Δt; the Earth rotated meantime with speed $\dot{S}$:

$$\Delta_{asc} = 2\pi R\cos\varphi \dot{S}\Delta t = 2\pi R\frac{\alpha}{\beta}\cos\varphi, \tag{7}$$

where $2\pi R\cos\varphi$ is the radius of a parallel circle at latitude $|\varphi|$, for $\varphi < I$ or $\varphi < 180^\circ - I$. The rotational speed of the Earth $\dot{S}$ (the angular rate) on the right hand side of Eq. (7) is in revolutions per day, thus equals 1.

Thanks to the resonance β/α, the orbit repeats during α days and the ascending points will be "densified" α-times (α is here a number, not the repeat period in days), so that

$$\Delta^{\alpha}_{asc} = \frac{\Delta_{asc}}{\alpha}.$$

The interval Δt "ascending-descending" during one revolution at latitude φ, let us denote it Δt_{da}, will be defined according to formula (6) and by means of Fig. 8. The mean anomaly $M_i = n\,t_i$ ($i = 1, 2$), measured from the equator for the ascending and descending points on a parallel φ can be rewritten as:

$$M_1 = nt_1 = \arcsin\frac{\sin\varphi}{\sin I}, \quad M_2 = nt_2 = \pi - \arcsin\frac{\sin\varphi}{\sin I},$$

where t_i are the instants of passing throughout the ascending and descending points on that parallel. Let us denote the relevant time interval between satellite passes through these two points $\Delta t_{da} = t_2 - t_1$. Then

$$\Delta t_{da} = t_2 - t_1 = \left(\pi - 2\arcsin\frac{\sin\varphi}{\sin I}\right)\frac{\alpha}{\beta}\frac{1}{2\pi}, \tag{8}$$

(in revolutions per day). For the turning points $|\varphi| = I$ or $180^\circ - I$, $\Delta t_{da} = 0$.

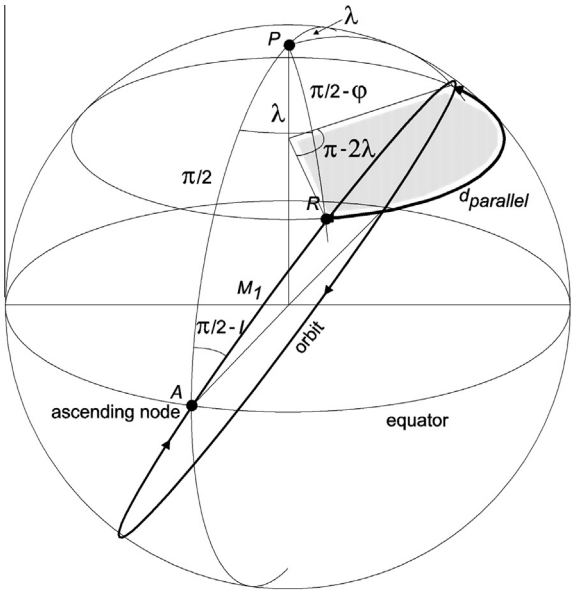

Fig. 8. Spherical geometry for the derivation of the distance between the ascending and descending tracks at latitude φ (Eq. (12)).

Let us denote the distance corresponding to the time interval Δt_{da}, on latitude φ, as d_{da}. It will consist of two components: (1) of a distance of the satellite flight around a hypothetical non-rotating Earth from the ascending to the descending points on that latitude, and (2) of a distance which is because the Earth rotates during satellite's flight from the ascending to the descending points (on the given parallel). Thus

$$d_{da} = 2\pi R\cos\varphi.(d_{parallel} - \dot{S}\Delta t_{da}), \tag{9}$$

where the units are: $d_{parallel}$ in a part of a circle (Fig. 8), Δt_{da} a part of a day, and d_{da} in [km].

To compute the distance d_{da}, we seek its part $d_{parallel}$. From Fig. 8, in the spherical triangle APR, we use the law of sines:

$$\sin\left(\frac{\pi}{2} - \varphi\right)\sin\lambda = \sin\left(\frac{\pi}{2} - I\right)\sin M_1,$$

$$\text{which yields} \qquad \cos\varphi\sin\lambda = \cos I\sin M_1,$$

$$\text{and then} \qquad \cos\varphi\sin\lambda = \cos I\frac{\sin\varphi}{\sin I},$$

$$\sin\lambda = \operatorname{cotg} I\cdot\operatorname{tg}\varphi,$$

$$\rightarrow \lambda = \arcsin\left(\frac{\operatorname{tg}\varphi}{\operatorname{tg} I}\right).$$

According to Fig. 8, we see that the distance on a parallel is proportional to $\pi - 2\lambda$ [in radians]. We express this angle as a part of a circle, thus

$$d_{parallel} = \frac{\pi - 2\lambda}{2\pi}, \tag{10}$$

where $d_{parallel}$ is in revolutions (the whole circle is 2π or 360° or 1 rev.).

For the distance d_{da-n} of the closest ascending and descending points, we then find

$$d_{da-n} = \mathrm{mod}(d_{da}, \Delta^{\alpha}_{asc}). \quad (11)$$

Let us denote $d_1 = d_{da-n}$, $d_2 = \Delta^{\alpha}_{asc} - d_{da-n}$, then the maximum distance d_{max} of the subsatellite points on the given latitude φ is

$$d_{max} = \max(d_1, d_2). \quad (12)$$

Eqs. (8), (9) and (12) are the main results till now. They do not change the "range" shown by the simple limit M_{max} (Eqs. (1a,b)), but provide details on the dependence of the actual limit in the individual satellite on latitude and inclination. Examples follow (Fig. 9 and others).

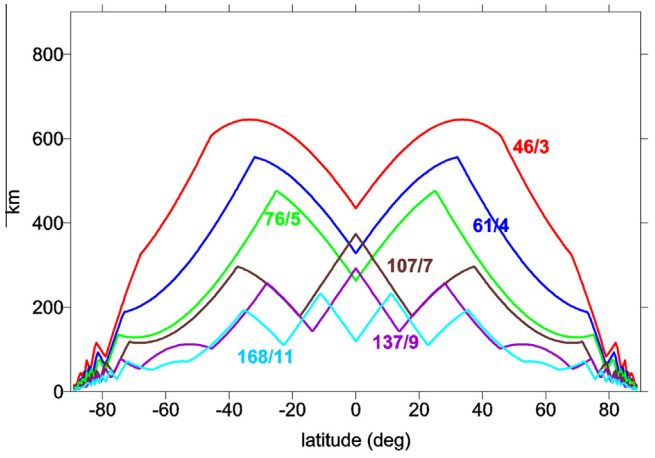

Fig. 9. Theoretical distance of the ground tracks d_{max} for GRACE, computed with Eq. (12) for the repeat orbits marked in Fig. 3.

2.5. Geometric interpretation of Eq. (12), the case of GRACE

First in Fig. 9 we plotted Eq. (12) for GRACE, showing the curves for the six repeat orbits marked in Fig. 3. Then in Fig. 10 we add a 3D diagram similar to Fig. 3 for an easy comparison, where the curves for the individual resonances are plotted also as a function of time.

We can see (Fig. 10) very good agreement between the theory (represented by Eqs. (8)–(12)) and "reality" (computed with the actual orbital elements in Fig. 3). We thus have a useful tool to understand the behavior of the rule (1a,b) and the distance defined by Eq. (12) which describes the dependence on latitude (strong dependence) and on inclination (a weak dependence) for the nearly polar orbits.

It is important to remember that the 3D diagram (Fig. 3) indicate the behavior away from the equator for various repeats; they clearly demonstrate that the distances based on the real data (Fig. 3) as well as the theoretical distances, computed according to Eq. (12), do not necessarily have their minima at the equator but sometimes (depending on the parity of $\beta - \alpha$) at lower latitudes, i.e. off the equator. This leads us back to Eq. (1a,b): with $(\beta - \alpha)$ odd, the minimum distance [of d_{max}] is at the equator and $M_{max} < \beta$ (if only the equator is considered); with $(\beta - \alpha)$ even, the minimum distance is away from the equator and $M_{max} < \beta/2$ (from the same consideration). However, Eqs. (1a,b) do not depend on latitude, they assume the track spacing is the same at every latitude. But we want to know the dependence of d_{max} on latitude and so judge M_{max} globally, not just at the equator.

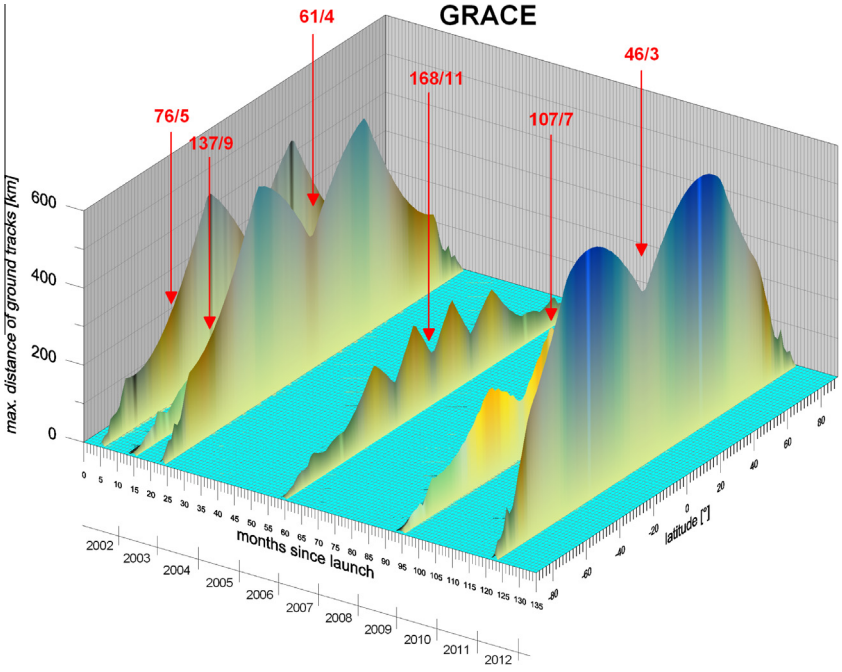

Fig. 10. 3D graph of evolution of theoretical ground track distances d_{max} for GRACE, computed with Eq. (12) for the resonances marked in Fig. 3. Maximal distance of the ground tracks is plotted as a function of time elapsed since the launch and of latitude. To be compared to Fig. 3.

2.6. Geometric interpretation of Eq. (12), GOCE

For GOCE, the situation is specific due to its fine orbit tuning which kept it at the selected repeats during the gradiometer measurement phases (see the list of resonances in Section 1, Table 2).

The results are given in Fig. 11 (a 2D graph for several selected repeats), using theoretical Eq. (12). In Figs. 12 and 13, 3D graphs show the evolution of the distances in time and as a function of latitude, computed again (as for GRACE) with the actual NASA two-line elements. The GOCE satellite after its launch was in free orbit decay from the initial height of about 280 km throughout the 16/1 repeat orbit to the 979/61 repeat, where the orbit was kept for gradiometry observations (Figs. 6 and 7). In Fig. 12, the 16/1 repeat is clearly marked (again we can test the theory given by Eq. (1a,b), not shown here). Further repeat orbits after the 16/1 revealed much smaller distances (much higher ground track density, smaller track separations), as predicted and expected, and to show their track density in more details we added Fig. 13. At the end of GOCE lifetime, just before its decay, a very irregular structure of the distances has appeared – the ion motor was not able to keep the orbit in the pre-selected repeat orbit of 2311/143, due to the enormous drag.

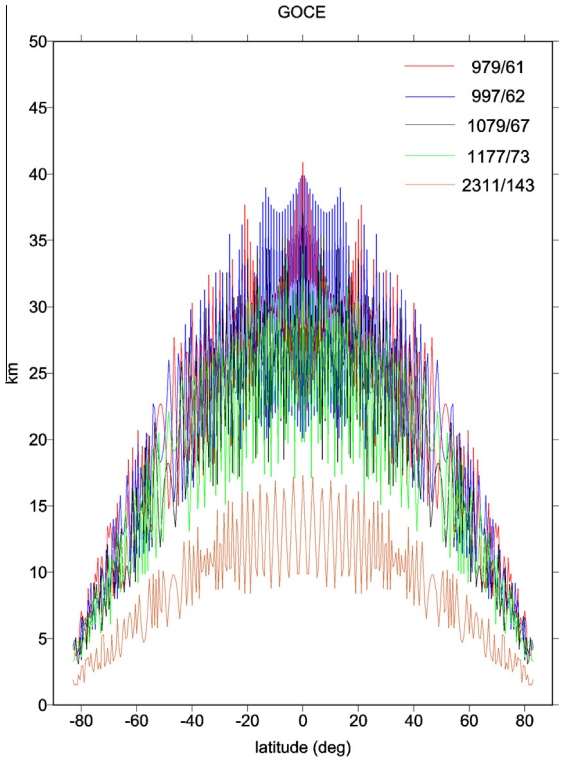

Fig. 11. Specific situation for GOCE. The theoretical distance of the ground tracks is shown here, as computed by Eq. (12), for five selected repeat orbits (from Table 2). Obviously, for such high variability with latitude (for large β), as for the repeat orbit 2311/143, the rule (1) becomes unimportant.

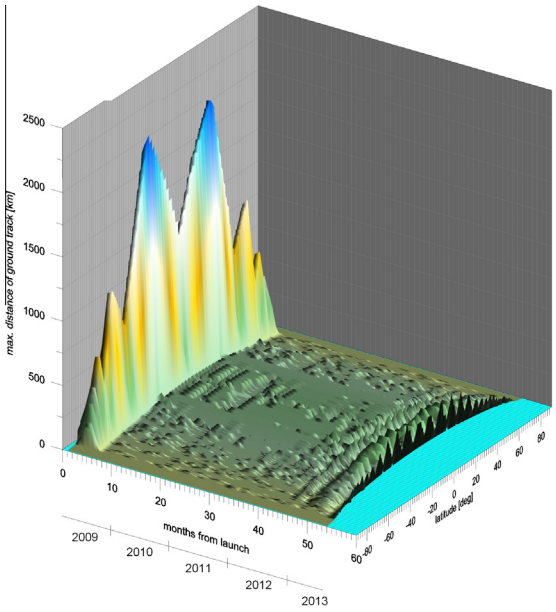

Fig. 12. 3D diagram similar to Fig. 3 for GRACE computed from NASA two-line elements, here for GOCE. The passage through the 16/1 repeat is a dominant feature of this plot. For further repeats after the 16/1, see Fig. 13.

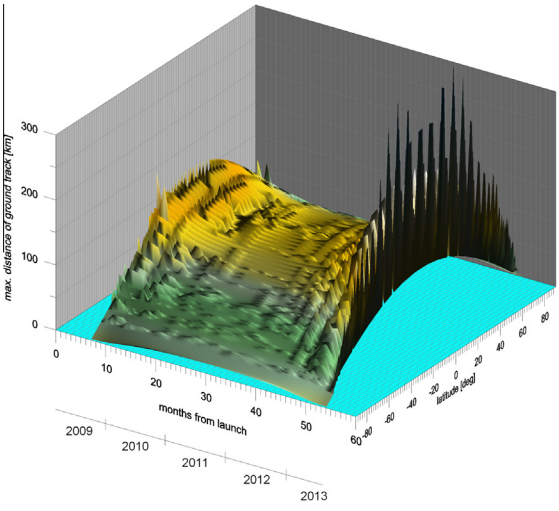

Fig. 13. 3D diagram similar to Fig. 3 based on the NASA two-line elements for GOCE. The passage through the 16/1 repeat is here omitted (see Fig. 12) and subsequent repeat regimes (taken from Table 2) are shown, nearly to the orbital decay of GOCE.

2.7. Effect of inclination

Since we believe that the best global resolution depends strongly on the global track density we need to go beyond the ground track figures and compute an "overall global track density" to find how it correlates with the overall error which we estimate for a given L_{max}, M_{max} and α, β with a variable orbit inclination I. We expect the optimal (smallest) overall error for this resolution to be reached with an inclination close to polar where the global track

density is greatest. One question is whether there is any significant difference for nearly polar prograde versus retrograde orbits.

The effect of inclination change on the shape of ground tracks is clearly shown by the series of Fig. 14a–e, where we compare the ground tracks of hypothetical orbits with inclinations 82°, 86°, ∼90°, 94°, and 98°, all at the 61/4 repeat orbit (as an arbitrary example).

What can be inferred from Fig. 14a–e? (i) The rule (1) is valid for both categories of the orbits (prograde as well as retrograde), but the shape of the ground tracks for them differs remarkably. Even a small change of inclination may induce a significant change of the global ground track geometry. (ii) For a prograde orbit the distance in latitude to where the crossings are reduced to 61 (in our case, equally spaced) is always greater than for its corresponding retrograde orbit. (iii) The prograde orbits evolve and cover the geographic space more slowly than the retrograde. Thus, a retrograde orbit covers a larger part of geographic space during the same time compared to its prograde

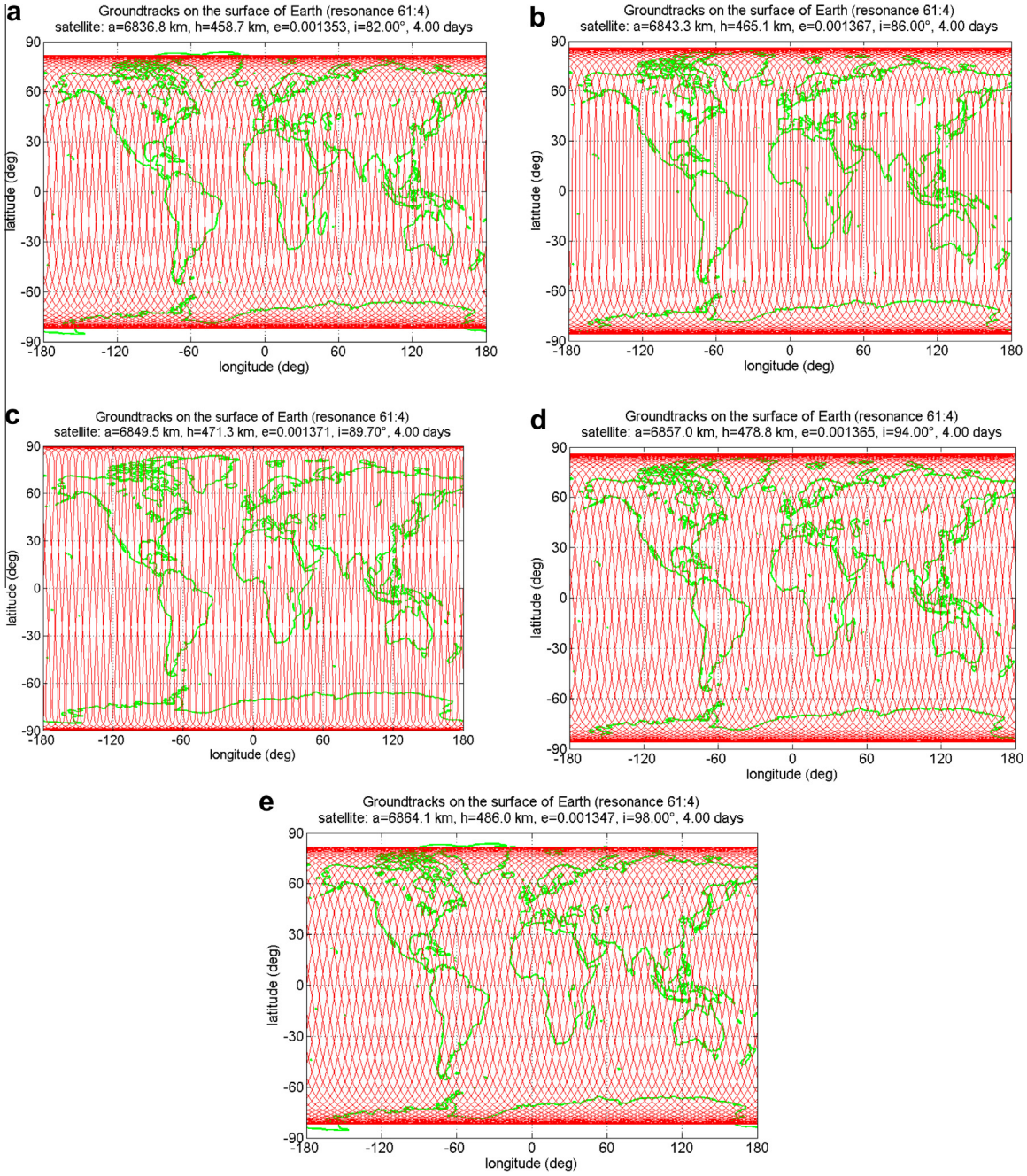

Fig. 14. (a–e) Ground tracks of five hypothetical satellites at inclinations 82°, 86°, ∼90°, 94°, and 98° at the 61/4 repeat, during an interval of 4 days. Note the different shape of the ground tracks for orbits with inclination symmetrical relative to 90° (in fact the "axis of symmetry" is not exactly at the polar orbit but close to $I = 86°$).

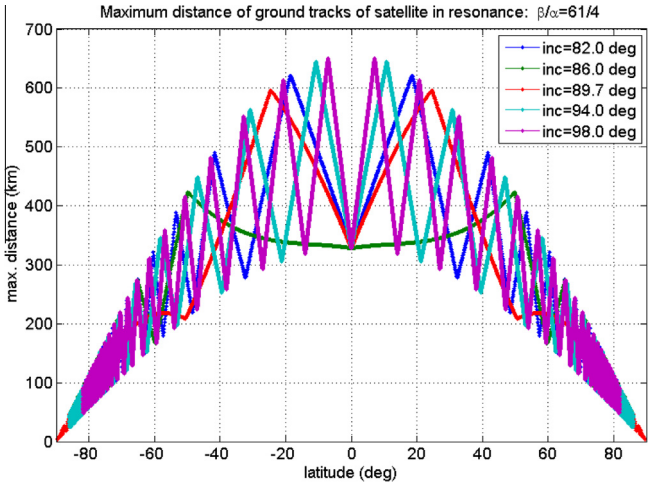

Fig. 15. The maximum ground track distances for the hypothetical satellites at inclinations 82°, 86°, ∼90°, 94°, and 98° at the 61/4 orbit (those with the ground tracks in Fig. 16a–e). We can see that the distances are similar for all nearly polar prograde as well as retrograde orbits (the case with $I = 86°$ is special, see Fig. 14b).

counterpart, which progresses in the same direction along with the Earth's rotation. (iv) All the 61/4 orbits start with maximum equally spaced crossings at the equator where the area coverage is most effective (the cosine of zero latitude is 1). But the prograde orbit changes its geographic coverage more slowly and reaches the minimum (least dense, equally spaced) crossing condition at higher latitudes than its retrograde pair, where the area covered is less effective (the cosine of latitudes are smaller).

And what about the density? The ground track density (and thus resolvability of the gravity field potential or its time variations) may differ for comparable prograde and retrograde orbits (both assumed nearly polar, in adequate distance from a reference polar orbit, as in Fig. 14a–e). Fig. 15 does not, however, confirm this expectation and shows that the global coverage is similar for all tested orbits.

3. Refinement of the rule for the limit M_{max}

The original Nyquist-type rule has been improved by Wagner et al. (2006) and Weigelt et al. (2009), as we already mentioned in *Introduction*. In this paper, we clearly demonstrated by Figs. 3, 12 and 13 (from the actual orbital data) and by Figs. 9–11 from the theory (the derivation leading to Eq. (12) in Section 2) that there is a dependence of the density of the ground tracks (and thus on the limit M_{max}) also on latitude and inclination, Eqs. (8), (9) and (12). Eqs. (1a,b) and (12) show that the limit M_{max} depends on the parity of $(\beta - \alpha)$ and will be somewhere between $\beta/2$ and β. Additionally, the smaller repeat revolutions β, the higher the dependence of M_{max} on latitude. Namely the lowest order repeat orbits (such as 31/2, 47/3, 61/4, ...) may substantially degrade solutions for their derived gravity field parameters.

Often filtering and additional constraints (a priori information) were used to overcome this problem, but this may compromise the solution. Another way is to seek a solution with "order dependent weighting" (lower weight for data near the low order exact resonance) used by Murboeck and Pail (2014). But they dealt with the temporal (not spatial) aliasing.

We claim that the correct solution is to decrease M_{max} temporarily in the vicinity of low order repeat orbits and to warn user against approaching situation which may be critical for some 1–3 months (see Fig. 3).

We wish to derive and use a limit for M_{max} sensitive to the global ground track density during these repeat conditions (not available by Eqs. (1a,b) which only account for the density at the equator). Specifically, we seek a continuous function for M_{max}, linear in an index of the global ground track density (defined below) yielding values between the 'natural' limits of β and $\beta/2$. The index we choose (for convenience) is the Average of the Maximum Distances (AMD) between adjacent ascending and descending passes along each sensed latitudinal band, as defined in Eq. (12). Note that the maximum of these distances occurs when the passes cross each other at a given latitude. The coverage density is least there (with maximum spacing), while it is greatest when each descending pass is midway between adjacent ascending ones (with minimum spacing). Therefore, we expect the sought M_{max}/AMD ratio to be negative (as AMD increases, M_{max} decreases while as AMD decreases, M_{max} increases).

To achieve a global assessment of AMD (within sensible latitudes) is easy for the theoretical extremes AMD_{max} (where ascending and descending passes overlap at all latitudes) and AMD_{min} (where the passes are equally spaced at all latitudes) but must be done numerically in latitude steps for the actual distances.

For the theoretical extremes, assume a polar orbit. The Ideal Maximum theoretical Distance (IMD_{max}) is:

$$IMD_{max} = \frac{2\pi}{\beta}\int_{-\pi/2}^{\pi/2} R\cos\varphi d\varphi = 2\frac{\pi}{\beta}R[\sin(\pi/2) - \sin(-\pi/2)] = 4\pi R/\beta, \quad (13)$$

and half this for IMD_{min}. Thus the AMD_{max} from pole to pole is:

$$AMD_{max} = IMD_{max}/\pi = 4R/\beta, \quad (14a)$$

and half this for AMD_{min}:

$$AMD_{min} = IMD_{min}/\pi = 2R/\beta. \quad (14b)$$

To find the M_{max} resolution as a linear function of the actual AMD note that at one extreme (all crossovers at every latitude), the evident Nyquist resolvable order M_{max} is $\beta/2$. At the other extreme (every latitude showing descending passes midway between neighboring ascending passes) the evident Nyquist resolvable order M_{max} is β. Therefore, given a measure of the actual track coverage

at every latitude as the maximum distance there between adjacent ascending and descending passes, how close is the average of these over the orbit's latitude limits (AMD computed numerically in latitude steps using Eq. (13)), to AMD_{min} or AMD_{max} (from Eqs. (14a,b)).

The two extremes of M_{max}, β and $\beta/2$, suggest the simple formulae for M_{max} as a linear function of AMD (note the negative ratio M_{max}/AMD forecast above):

$$M_{max} = (\beta/2)[3 - \beta AMD/(2R)]. \quad (15)$$

When $AMD = AMD_{min} = 2R/\beta$ (Eq. (14b)), $M_{max} = \beta$ (one extreme for Nyquist pole to pole coverage). Similarly, when $AMD = AMD_{max} = 4R/\beta$ (Eq. (14a)), $M_{max} = \beta/2$ (the other extreme for Nyquist coverage). Thus Eqs. (1a,b) correspond to ideal (theoretical) maximum and minimum track density coverage.

Limits for the new Eq. (15) which is continuous and linear in the actual global track coverage AMD, depends also (and strongly) on latitude and the inclination of the orbit (assumed to be nearly but not necessarily exactly polar).

A few examples for M_{max} computed with Eq. (15) for CHAMP, GRACE and GOCE are given in Table 3 (compare to Table 1).

We can see by comparing Tables 1 and 3 that for example for the 61/4 orbit, Eq. (1a,b) predicts the limit $M_{max} = 61$ and here, with the refined rule, Eq. (15), we have M_{max} only 43. On the contrary, while the rule (1) yields $M_{max} = 54$ for the 107/7, the rule (15) gives a global track density estimate of $M_{max} = 77$.

Fig. 16 shows the above results for M_{max} compared to the extremes (β and $\beta/2$) for the GRACE and CHAMP repeat orbits. Note especially that while the majority of these repeat orbits give M_{max} closer to β, when β and α have different parity (empty symbols) or closer to $\beta/2$, when the parities are the same (filled symbols in Fig. 16) this is not true for all of them. The GRACE resonances in particular show M_{max} estimates all close to the average of β and $\beta/2$ with some violating the expectation from Eqs. (1a,b), using just the equatorial distances as the criteria for M_{max}.

Rather than use the pole-to-pole values of IMD_{max} in Eq. (13), we could compute them as integrated between the actual limits of φ for the particular satellite. However since the actual repeat orbits are always close to polar,

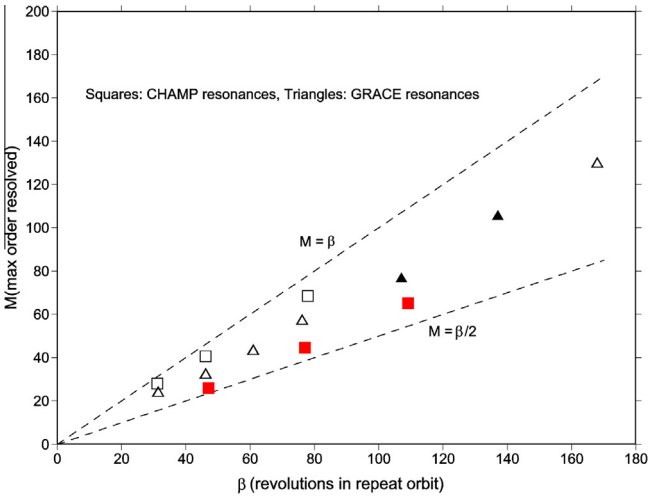

Fig. 16. Estimate of resolvable order M_{max} versus order β in an (β/α) repeat orbit. Filled symbols have (α, β) of the same parity.

the differences in the resulting M_{max} are small, not more than two orders. The theoretical (pole to pole) solution is preferred because it does not lose the connection to the Nyquist criteria which require an integration from pole to pole.

A comparison of M_{max} from Table 3 with results for the 46/3 and 47/3 repeats in Weigelt et al. (2013) reveals some discrepancies which can be explained by totally different approaches – any rule based only on track density will only provide a "generalized" or "smoothed" value, while an inversion of actual data (for a given repeat orbit) shows (for example by means of the inverses condition numbers or correlation coefficient matrix) the preferred resolution for a particular case.

4. Conclusions

One of the limiting factors in the determination of gravity field parameters is the spatial sampling, namely during phases when the satellite is in a low order repeat (resonant) orbit. The ground track density in such a situation decreases and large data gaps appear in the coverage of the globe. In turn, gravity field parameters derived under such conditions (for a free drifting satellite in the upper

Table 3
Resolution M_{max} for the three satellites, using Eq. (15), together with AMD values.

Satellite	CHAMP ($I = 87.2°$)			GRACE ($I = 89.0°$)			GOCE ($I = 96.7°$)		
	β/α	AMD [km]	M_{max}	β/α	AMD [km]	M_{max}	β/α	AMD [km]	M_{max}
	46/3	336	42	76/5	251	58	979/61	21	730
	77/5	304	47	137/9	135	107	997/62	21	750
	31/2	485	29	61/4	334	43	1079/67	19	800
	78/5	204	69	168/11	111	131	1177/73	17	885
	47/3	512	26	107/7	186	78	2311/143	9	1740
	109/7	241	68	46/3	448	32			
				31/2	591	24			

atmosphere) lose accuracy. This phenomenon is inevitable but fortunately only temporal (short in a comparison with other phases of satellite's flight on freely decaying orbit, see Fig. 3 along the x-axis).

The problem has been intensively studied (Wagner et al., 2006; Klokočník et al., 2008; Weigelt et al., 2009, 2013) and simple rules have been derived for the maximum order for objective determination of the gravity field parameters (mainly their time variations). We worked here with the rule taken from Weigelt et al. (2013), see Eqs. (1a,b), which distinguishes the maximum recommended order for the gravity parameters determination according only to the parity of the two parameters (α, β) defining the relevant repeat orbit. We demonstrate clearly that and how latitude and inclination affects the choice of the limit based on the global track coverage, not just the coverage at the equator.

The simplest rationale for the $M_{max} < \beta$ rule (for band limited resolutions, it means $M_{max} = L_{max}$) comes from the twice as common $(\beta - \alpha)$ odd repeat orbits where on the equator there are 2β equally spaced crossings in 360° of longitude or two crossings to determine the minimum $M_{max} = \beta$ wave. But at other latitudes (where the ascending and descending crossings are at the same longitudes), an $M_{max} = \beta/2$ rule is more appropriate. This suggests that a better rule from track density only should provide results somewhere between $M_{max} = \beta/2$ and $M_{max} = \beta$. It was derived and presented in Section 3 as Eq. (15), which is continuous and linear in the actual global track coverage, dependent directly on geopotential order β and indirectly on latitude and inclination.

We emphasize that the estimate of M_{max} resolvability from Eq. (15) is only a first estimate easily made without resort to inversions of actual or proposed data errors and sampling protocols. We consider it a fair compromise between the long held Colombo (1984) and recently revisited (2013) Weigelt rule.

Although our findings are new and explain various facts previously hidden, we are well aware that the problem of the influence of insufficient spatial sampling on the quality (in errors) of a gravity field determination is not directly addressed here. Our global "geometric approach" used to estimate maximum resolution has to be supplemented by a "dynamic approach", using practical inversions from the particular data to the gravity field parameters. Their results may differ from the theory presented here, because no rule can describe real gravity errors in detail.

Acknowledgments

We are grateful for grant provided by GA ČR #13-36843S, programme RVO 67985815, and for the project of the European Regional Development Fund (ERDF) "NTIS – New Technologies for Information Society", European Centre of Excellence, CZ.1.05/1.1.00/02.0090 for the Czech co-authors. We thank M. Weigelt PhD for Fig. 5 and Dr S. Bettadpur for Fig. 1.

References

Allan, R.R., 1973. Satellite resonance with longitude-dependent gravity—III, inclination changes for close satellites. Planet. Space Sci. 21, 205–225.

Awange, J.L., Sharifi, M.A., Ogonda, G., et al., 2008. The falling Lake Victoria water level: GRACE, TRIMM and CHAMP satellite analysis of the lake basin. Water Resour. Manage. 22 (7), 775–796. http://dx.doi.org/10.1007/s11269-007-9191-y.

Bettadpur, S., 2008. Orbital mechanics, perturbations and GRACE science and mission design. In: Seago, J.H., Neta, B., Eller, T.J., et al. (Eds.), Conference: AAS/AIAA 18th Space Flight Mechanics Meeting, Galveston, TX, USA. Jan 28–Feb 01, Amer. Astronaut Soc., Amer. Inst. Aeronaut. & Astronaut. AAS 08-179.

Bettadpur, S., Poole, S., Ries, J., 2004. GRACE mission status and gravity field product improvement plans. Paper G23-A01, AGU Fall Meeting 2004.

Bezděk, A., Klokočník, J., Kostelecký, J., Floberghagen, R., Gruber, C., 2009. Simulation of free fall and resonances in the GOCE mission. J. Geodyn. 48, 47–53. http://dx.doi.org/10.1016/j.jog.2009.01.007.

Bezděk, A., Klokočník, J., Kostelecký, J., Floberghagen, R., Sebera, J., 2010. Some aspects of the orbit selection for the measurement phases of GOCE. In: Proceedings of the ESA Living Planet Symposium, ESA SP-686, Bergen, Norway, 28 June–2 July.

Colombo, O., 1984a. Altimetry, orbits and tides, NASA Tech. Memo. 86180, Goddard Space Flight Center, Greenbelt, 173 pp.

Colombo, O., 1984b. The global mapping of gravity with two satellites. In: Netherl. Geod. Comm., Publ on Geodesy 7(3). <http://www.ncg.knaw.nl/eng/publications/geodesy.html>.

Elsaka, B., Raimondo, J.C., Brieden, P., et al., 2014. Comparing seven candidate mission configurations for temporal gravity field retrieval through full-scale numerical simulation. J. Geod. 88, 31–43. http://dx.doi.org/10.1007/s00190-013-0665-9.

ESA, 1999. Gravity field and steady-state ocean circulation mission – Report for mission selection. ESA Report SP-1233(1). <http://earth.esa.int/goce04/Documents/goce_sp1233_1.pdf>.

ESA, 2014. GOCE End-of Mission Operations Report, GOCE Flight Control Team, document GO-RP-ESC-FS-6268. <https://earth.esa.int/documents/10174/85857/2014-GOCE-Flight-Control-Team.pdf>.

Floberghagen, R., Fehringer, M., Lamarre, D., Muzi, D., Frommknecht, B., Steiger, C., Pineiro, J., da Costa, A., 2011. Mission design, operation and exploitation of the gravity field and steady-state ocean circulation explorer mission. J. Geod. 85, 749–758. http://dx.doi.org/10.1007/s00190-011-0498-3SATELLTE.

Gooding, R.H., 1971. Lumped fifteenth-order harmonics in the geopotential. Nat. Phys. Sci. 231, 168–169. http://dx.doi.org/10.1038/physci231168a0.

Kaula, W.M., 1966. Theory of Satellite Geodesy. Blaisdell, Massachusetts, USA.

Klokočník, J., Kostelecký, J., 2006. Degradation in accuracy of gravity variations from CHAMP, GRACE, and GOCE. In: Presented at 3rd Int. GOCE user workshop, November, ESA-ESRIN, Frascati, Italy, CD, ESA.

Klokočník, J., Kostelecký, J., Gooding, R.H., 2003. On fine orbit selection for particular geodetic and oceanographic missions involving passage through resonances. J. Geod. 77, 30–40.

Klokočník, J., Wagner, C.A., Kostelecký, J., Bezděk, A., Novák, P., Mcadoo, D., 2008. Variations in the accuracy of gravity recovery due to ground track variability: GRACE, CHAMP, and GOCE. J. Geod. 82, 917–927. http://dx.doi.org/10.1007/s00190-008-0222-0.

Klokočník, J., Bezděk, A., Kostelecký, J., Sebera, J., 2010. Orbit tuning of planetary orbiters for accuracy gain in gravity-field mapping. J. Guid. Control Dyn. 33 (3), 853–861. http://dx.doi.org/10.2514/1.46223.

Klokočník, J., Bezděk, A., Kostelecký, J., 2011. GNSS-R concept extended by a fine orbit tuning. Adv. Space Res. 49, 957–965. http://dx.doi.org/10.1016/j.asr.2011.12.008.

Klokočník, J., Gooding, R.H., Wagner, C.A., Kostelecký, J., Bezděk, A., 2013. The use of resonant orbits in satellite geodesy: a review. Surv. Geophys. 34, 43–72. http://dx.doi.org/10.1007/s10712-012-9200-4, ISSN 0169-3298.

Lemoine, J.-M., Bruinsma, S., Loyer, S., Biancale, R., Marty, J.-C., Perosanz, F., Balmino, G., 2007. Temporal gravity field models inferred from GRACE data. Adv. Space Res. 39, 1620–1629.

Murboeck, M., Pail, R., 2014. De-correlated combination of two low–low satellite-to-satellite tracking pairs according to temporal aliasing. Geophysical Research Abstracts 16, EGU2014-11175, EGU Vienna 2014.

Ramillien, G., Biancale, R., Gratton, S., Vasseur, X.S., Bourgogne, S., 2011. GRACE-derived surface water mass anomalies by energy integral approach: application to continental hydrology. J. Geod. 85, 313–328. http://dx.doi.org/10.1007/s00190-010-0438-7.

Ramillien, G., Seoane, L., Frappart, F., Biancale, R., Gratton, S., Vasseur, X., Bourgogne, S., 2012. Constrained regional recovery of continental water mass time-variations from GRACE-based geopotential anomalies over South America. Surv. Geophys. 33, 887–905. http://dx.doi.org/10.1007/s10712-012-9177-z.

Reigber, Ch., Klokočník, J., Li, H., Flechtner, F., 1988. Orbit dossier. Contribution to ERS-1, German PAF.

Reigber, C., Luhr, H., Schwintzer, P., 2002. CHAMP mission status. Adv. Space Res. 30 (2), 129–134.

Rosborough, G., 1986. Satellite orbit perturbations due to the geopotential, CSR-86-1 report, pp. 154, Center for Space Research, The university of Texas at Austin, Austin, USA.

Save, H., Bettadpur, S., Tapley, B.D., 2012. Reducing errors in the GRACE gravity solutions using regularization. J. Geod. 86, 695–711. http://dx.doi.org/10.1007/s00190-012-0548-5.

Schmidt, M., Seitz, F., Shum, C.K., 2008. Regional four-dimensional hydrological mass variations from GRACE, atmospheric flux convergence, and river gauge data. J. Geophys. Res. 113, B10402. http://dx.doi.org/10.1029/2008JB005575.

Seitz, F., Schmidt, M., Shum, C.K., 2008. Signals of extreme weather conditions in Central Europe in GRACE 4-D hydrological mass variations. Earth Planet. Sci. Lett. 268, 165–170. http://dx.doi.org/10.1016/j.epsl.2008.01.001.

Swenson, S., Yeh, P.J.F., Wahr, J., et al., 2006. A comparison of terrestrial water storage variations from GRACE with in situ measurements from Illinois. Geophys. Res. Lett. 33 (16), L16401. http://dx.doi.org/10.1029/2006GL026962.

Tapley, B., Bettadpur, S., Watkins, M., Reigber, Ch., 2004. The gravity recovery and climate experiment: mission overview and early results. Geophys. Res. Lett. 31, L09607. http://dx.doi.org/10.1029/2004GL010020.

Visser, P.N.A.M., Sneeuw, N., Reubelt, T., Losch, M., van Dam, T., 2010. Space-borne gravimetric satellite constellations and ocean tides: aliasing effects. Geophys. J. Int. 181 (2), 789–805. http://dx.doi.org/10.1111/j.1365-246X.2010.04557.x.

Visser, P.N.A.M., Schrama, E.J.O., Sneeuw, N., Weigelt, M., 2012. Dependency of resolvable gravitational spatial resolution on space-borne observation techniques. In: Kenyon, S., Pacino, M., Marti, U. (Eds.), Geodesy for Planet Earth: Proceedings of the 2009 IAG Symposia Buenos Aires, Argentina. Springer, Berlin, pp. 373–379. http://dx.doi.org/10.1007/978-3-642-20338-1_45, vol. 136.

Wagner, C., McAdoo, D., 2004. Time variations in the GRACE gravity field: constraints on global hydrologic mass flux. In: Reigber, Ch., Tapley, B. (Eds.), Proc Joint CHAMP/GRACE Sci Meet, GFZ Potsdam, 6–8 July.

Wagner, C.A., Mcadoo, D., Klokočník, J., Kostelecký, J., 2006. Degradation of geopotential recovery from short repeat-cycle orbits: application to GRACE monthly fields. J. Geod. 80, 94–103. http://dx.doi.org/10.1007/s00190-006-0036-x.

Weigelt, M., Sneeuw, N., Keller, W., 2008. Evaluation of EGM2008 by comparison with global and local gravity solutions from CHAMP. In: Mertikas, IAG Symp. 135: 497504 (publ. in 2010), doi: 10.1007/978-3-642-10634-7_19.

Weigelt, M., Sideris, M.G., Sneeuw, N., 2009. On the influence of the ground tracks on the gravity field recovery from high–low satellite-to-satellite tracking missions: CHAMP monthly gravity field recovery using the energy balance approach revisited. J. Geod. 83, 1131–1143. http://dx.doi.org/10.1007/s00190-009-0330-5.

Weigelt, M., Antoni, M., Keller, W., 2010. Regional gravity field recovery from GRACE using position optimized radial base functions. IAG Symp. 135, 139–146. http://dx.doi.org/10.1007/978-3-642-10634-7_19.

Weigelt, M., Sneeuw, N., Schrama, E.J.O., Visser, P.N.A.M., 2013. An improved sampling rule for mapping geopotential functions of a planet from a near polar orbit. J. Geod. 87, 127–142. http://dx.doi.org/10.1007/s00190-012-0585-0.

Wiese, D.N., Nerem, R.S., Lemoine, F.G., 2012. Design considerations for a dedicated gravity recovery satellite mission consisting of two pairs of satellites. J. Geod. 86, 99–108. http://dx.doi.org/10.1007/s00190-011-0494-7.

Zaitchik, B.F., Matthew, R., Reichle, R.H., 2008. Assimilation of GRACE terrestrial water storage data into a land surface model: results for the Mississippi river basin. J. Hydrometeorol. 9, 535–548. http://dx.doi.org/10.1175/2007JHM951.1.